An improved statistical wake meandering model

Journal of Physics: Conference Series **2767** (2024) 092048 doi:10.1088/1742-6596/2767/9/092048

An improved statistical wake meandering model

Peter Brugger[1], **Corey Markfort**[2], **Fernando Porté-Agel**[1]

[1] Wind Engineering and Renewable Energy Laboratory (WiRE), École Polytechnique Fedérale de Lausanne (EPFL), 1015 Lausanne, Switzerland
[2] IIHR-Hydroscience & Engineering, Dept. of Civil and Environmental Engineering, The University of Iowa, Iowa City, IA 52242, USA

E-mail: peter.brugger@epfl.ch

Abstract. A new statistical wake meandering (SWM) model is proposed that improves on existing models in the literature. Compared to the existing SWM models, the proposed model has a closed description that does not require simulations to create look-up tables while maintaining applicability to a wide range of flow conditions. The proposed SWM model is compared to the predictions of the Dynamic Wake Meandering (DWM) model and to wind speed measurements from a scanning Doppler lidar mounted on the nacelle of a utility-scale wind turbine for validation. The results show that the proposed model has a similar performance as the DWM model for the effect of wake meandering on the mean velocity deficit and the turbulence intensity, while being significantly faster to compute.

1. Introduction

Wind turbine wakes impinging on other wind turbines within a wind farm are a significant source of power losses and they decrease the lifetime of affected wind turbines. Wake meandering is a low-frequency spanwise oscillation of the entire wake for which large-scale turbulence of the inflow is assumed to be a dominant driver (Fig. 1) [17]. It affects power production of wind farms due to its impact on the velocity deficit recovery, and it affects loads due to the turbulence added to the downstream flow [13]. Therefore, the modelling of wake meandering is one important aspect of wind farm development. However, simulations resolving all relevant turbulent length scales are still too computationally costly for iterative wind farm design tools [4].

Computationally fast modelling approaches for wake meandering are the Dynamic Wake Meandering (DWM) model [13] and statistical wake meandering (SWM) models [11, 18, 4]. The DWM model operates on the assumption that the wake behaves like a passive tracer that is transported as a whole by the large-scale turbulence of the atmosphere (Fig. 1). The DWM model solves the shear-layer equations [1] for the velocity deficit, which is assumed to be steady in a meandering frame of reference (MFoR) following the instantaneous wake center position. The wake meandering is then described by displacing the quasi-steady velocity deficit in the lateral and vertical direction along the pathlines of the low-pass filtered velocity field originating from the wind turbine. These pathlines require the DWM model to be coupled with another model for the background flow field like e.g. an aerolastic solver. The underlying passive-tracer assumption of the DWM model has been validated with some minor modifications [3, 19, 14, 5].

Statistical wake meandering (SWM) models further simplify the modelling framework of the DWM model by replacing the pathlines with a probability density function (PDF) of the instantaneous wake center position. This removes the need for coupling with external models

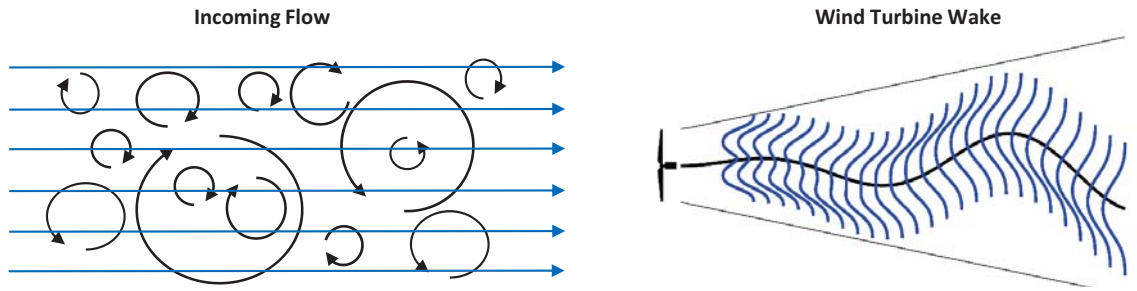

Figure 1. Illustration of wake meandering at an isolated wind turbine. Large-scale turbulence of the inflow (left) displaces the wake of a wind turbine in the spanwise direction (right). The quasi-steady velocity deficit in the meandering frame of reference is indicated in blue and the wake center displacement in black. Figure reused from [6] under the Creative Commons Attribution 4.0 License (https://creativecommons.org/licenses/by/4.0/).

for the background flow field, which is the reason why they are also referred to as standalone DWM model in [11], at the cost of the spectral information that the DWM model can provide. They retain the modelling framework of the DWM model consisting of three parts: (i) a quasi-steady velocity deficit in the MFoR, (ii) a lateral and vertical displacement of the quasi-steady velocity deficit due to the large-scale turbulence of the boundary layer, and (iii) a method that combines (i) and (ii) for predictions of the mean wind field and the turbulence in the fixed frame of reference (FFoR). Currently, there are three different SWM models in the literature, namely the Keck model [11], the Thøgersen et al. model, [18], and the Braunbehrens and Segalini model [4]. An overview of them is presented in Table. 1.

As can be seen from Table. 1, the existing SWM models each use different methods with their own drawbacks and benefits. While the Thøgersen et al. [18] model is easy to implement and fast to compute, it fails to capture the influence of ambient flow conditions on the wake meandering. While the Braunbehrens and Segalini model [4] and the Keck model [11] lead to more realistic results compared to the Thøgersen et al. model, their set up requires look-up tables created from prior simulations and they do not include a realistic prediction of the turbulence intensity (the latter will be shown in section 2.3). Therefore, we believe there is a need for an improved SWM model that addresses those issues.

Here, we want to propose a further iteration of a SWM model that has a closed model description like the Thøgersen et al. model [18], while maintaining the applicability to a wide-range of flow states like the Keck model and the Braunbehrens and Segalini model. Further, we want to improve the predictions of the turbulence intensity added by wake meandering compared to previous SWM models. The paper is structured as follows: section 2 describes the proposed model, section 3 describes the measurements used for the model validation, section 4 presents the validation results, and we close with our conclusions in section 5.

2. Statistical wake meandering model

The proposed statistical wake meandering model can be divided into three parts: First, the quasi-steady velocity deficit is modelled with an adapted analytical wake model. Second, a PDF of the instantaneous wake center positions for a given flow state and downstream distance is created. And lastly, an ensemble of quasi-steady velocity deficits is created according the PDF and the mean velocity field and added turbulence intensity are derived from its statistics. Each part is detailed in the following subsections.

Table 1. Overview of statistical wake meandering models in the literature and the here proposed model. The table details the three principal components of each model (rows two to four) and highlights differences to the here proposed model (bottom row).

Authors	Keck (2015) [11]	Thøgersen et al. (2017) [18]	Braunbehrens and Segalini (2019) [4]	Proposed model
Quasi-steady velocity deficit in the MFoR	Axis-symmetric shear-layer equations [1] using mean wind speed, turbulence intensity, and axial induction factor as input.	Top-hat shaped wake from analytical Jensen model [10] using a small wake growth rate and mean wind speed as input.	Gaussian shaped wake from look-up table generated from solving linearised Naviar-Stokes equations with actuator disk for several flow configurations.	Gaussian shaped wake from analytical wake model [2] using a small wake growth rate and mean wind speed, turbulence intensity, and thrust-coefficient as input.
PDF of the instantaneous wake center position	Look-up table for meandering PDF generated from simulations for several ambient flow conditions.	Axis-symmetric PDF independent of ambient conditions.	Normal distribution scaled with the friction velocity and the integral time scale (vertical meandering set to half of the lateral).	Normal distribution scaled with turbulence intensity, and mean wind speed (vertical meandering set to 0.6-0.9 of the lateral).
Model output and combination method	Mean velocity field and turbulence intensity computed from convolution of the meandering PDF and the quasi-steady velocity deficit.	Mean velocity deficit from ensemble average.	Mean velocity field computed from convolution of the meandering PDF and the quasi-steady velocity deficit.	Mean velocity deficit from ensemble average and added turbulence intensity from ensemble standard deviation.
Key differences between existing models and the proposed model	Requires simulations to create look-up table and the method to compute the turbulence intensity leads to unrealistic results.	Very fast and simplistic model, but a major drawback is missing the influence of the ambient turbulence intensity on the wake meandering strength.	Does not provide the turbulence intensity and requires simulations to create look-up tables.	Accounts for influence of ambient flow without look-up tables generated from simulations and provides the mean velocity field and the added turbulence intensity.

2.1. Quasi-steady velocity deficit

Inspired by Thøgersen et al. [18], we also use an analytical model for the quasi-steady velocity deficit in the MFoR (ΔU_{qs}). This has the benefit of faster computation times compared to the Keck model [11] and not requiring simulations to be done in advance like for the Braunbehrens and Segalini model [4]. The quasi-steady velocity deficit in MFoR has been shown to be of Gaussian shape beyond a certain downstream distance [16]. Therefore, we propose to use the analytical model of Bastankhah and Porté-Agel [2] with a wake growth rate that only accounts for the turbulence created by the wake itself. It is given by:

$$\frac{\Delta U_{qs}(x,y,z)}{U_0(z)} = \left(1 - \sqrt{1 - \frac{C_T}{8\sigma_w^2(x)D^{-2}}}\right) e^{-0.5y^2\sigma_w^{-2}(x)} e^{-0.5z^2\sigma_w^{-2}(x)} \tag{1}$$

where U_0 is the incoming mean wind speed, C_T is the thrust coefficient of the wind turbine, D is the rotor diameter, y (z) is the lateral (vertical) coordinate with origin at the turbine nacelle, and the σ_w is the wake width given by

$$\sigma_w = k^*_{MFoR}(x - x_0) + \frac{D}{\sqrt{8}}, \tag{2}$$

where $k^*_{MFoR} = 0.021$ is the wake growth rate in the MFoR chosen to account only for the self induced wake growth based on observed wake growth rates at very low ambient turbulence levels from LES [2], and the near-wake length is given by

$$x_0 = \frac{(1 + \sqrt{1 - C_T})D}{\sqrt{2}(\alpha TI_u + \beta(1 - \sqrt{1 - C_T}))}, \tag{3}$$

where TI_u is the streamwise turbulence intensity of the inflow at hub height, $\alpha = 3.6$, and $\beta = 0.154$. Figure. 2a shows that the resulting quasi-steady velocity deficit agrees well with the results obtained by solving the shear-layer equations for large x, but overestimates the amplitude for small x. We consider this as acceptable because turbine spacing in wind farms is typically larger than $5D$ and Eq. 1 is an order of magnitude faster to compute (or more for a larger grid). A dependency of the amplitude of the quasi-steady velocity deficit in the MFoR to the turbulence intensity as reported in [16] is reproduced with Eq. (1) due to x_0 decreasing with TI_u, but the dependency is stronger than in their data. The choice of a Gaussian shape for the quasi-steady velocity deficit and Eq. (3) for the near-wake length is further justified by Fig. 2b, which shows the onset of a Gaussian shaped quasi-steady velocity deficit from observations. Equation (3) provides a reasonable approximation of $x_{0,MFoR}$ even though it was designed for the FFoR and not the MFOR. We applied the quasi-steady velocity deficit that is determined at $x_{0,MFoR}$ also to $x < x_{0,MFoR}$, which leads to unrealistic results at short downstream distances inside the near-wake.

2.2. Probability density function of the instantaneous wake center position

The PDF of the instantaneous wake center position is designed to account for the most important effects of the ambient flow on wake meandering. These are an increase of the wake meandering strength with the ambient turbulence intensity and with the downstream

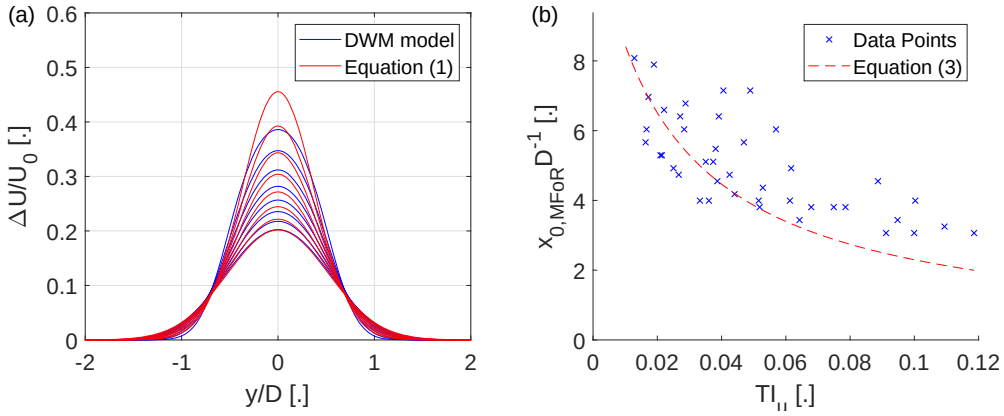

Figure 2. Comparison of quasi-steady velocity deficit in the MFoR between Eq. (1) in red and the shear-layer equations [1] used by the DWM model in blue (a). Results shown between $x = 3D$ (highest curves) and $x = 10D$ (lowest curves) in $1D$ increments and the models where initialised with $U_0 = 5$ m s^{-1}, $TI_u = 0.12$, $C_T = 0.8$, and $D = 96$ m. The right panel (b) shows the onset of a Gaussian shaped wake in the MFoR quantified as the first downstream distance with an $R^2 > 0.95$ for a Gaussian fit [7]. The data set and the transformation into the MFoR are from [5].

distance from the wind turbine [8, 14, 5]. The PDF for the lateral wake position is modelled with a normal distribution given by

$$PDF_m(x, y) = \frac{1}{\sqrt{2\pi}\sigma_{m,y}(x)} e^{-\frac{1}{2}\left(\frac{y}{\sigma_{m,y}(x)}\right)^2}, \tag{4}$$

where the width of the meandering distribution is modelled with

$$\sigma_{m,y}(x) = \frac{1}{2} TI_{v,f} x, \tag{5}$$

where $TI_{v,f}$ is the low-pass filtered turbulence intensity with filter threshold of $2D$ to reflect that only the large-scale turbulence contributes to the wake meandering. The assumption of a linear relationship between wake meandering strength and the downstream distance is based on experimental data [5] and the scaling factor was chosen empirically to provide good agreement in the validation. It has been suggested that the linear increase of the wake meandering strength changes to a square-root growth at large downstream distances ($x > 10D$) [4]. However, our data availability for the validation in section 4 is scarce for $x > 9D$ and we cannot investigate this therefore.

The PDF for the vertical wake position also follows Eq. (4) with a modified width given by $\sigma_{m,z}(x) = c_{yz}\sigma_{m,y}(x)$ where the ratio of lateral to vertical wake meandering is given by $c_{yz} = 0.8$, which has been suggested for neutral stratification [12]. This is larger than the value of 0.5 used by the Braunbehrens and Segalini model [4] and there is no consensus on its value or its dependency with the stratification in the literature.

2.3. Velocity deficit and turbulence intensity in the fixed frame of reference

Lastly, the PDF of the wake center position (Eq. 4) needs to be combined with the quasi-steady velocity deficit (Eq. 1) to model the mean velocity deficit and the added turbulence

intensity. We use an ensemble average of the spatially displaced quasi-steady velocity deficits to compute the mean velocity deficit given by

$$\Delta U_{avg}(y,z) = \langle \Delta U_{qs}(y - y_m, z - z_m) \rangle \tag{6}$$

with y_m and z_m drawn randomly from PDF_m, and $\langle ... \rangle$ is the ensemble average. For the added turbulence intensity due to wake meandering, the ensemble standard deviation given by

$$TI_{std}(y,z) = \sqrt{\langle \Delta U_{qs}(y - y_m, z - z_m) - \Delta U_{avg}(y,z) \rangle^2} U_0^{-1} \tag{7}$$

is used. A convolution approach that is computationally faster exists in literature [11], but it led to unrealistic results for the added turbulence intensity (not shown).

3. Research site and measurements

The test site is an isolated 2.5 MW Liberty C96 wind turbine form Clipper Windpower (hub height of 79 m and a rotor diameter of 96 m) at the Kirkwood Community Collage in Cedar Rapids, Iowa. Measurements were conducted over one month in autumn 2017. The supervisory control and data acquisition (SCADA) of the wind turbine provided the wind speed at hub height averaged over 10-minute periods (U_0). The measurement uncertainty of U_0 is assumed to be 0.25 m s^{-1} based on a comparisons to the Doppler LiDAR measurements (not shown).

Two pulsed Doppler Light Detection and Ranging (LiDAR) systems were mounted on the roof of the nacelle (Fig. 3a). A Doppler LiDAR measures the line-of-sight velocity of the air along a laser beam that is emitted by the instrument. The instruments were Stream Line models from Halo Photonics Ltd. (Worecestershire, UK). The Doppler LiDARs sampled the velocity with a temporal frequency of 3 Hz and spatial resolution of 18 m along the laser beam.

The Doppler LiDAR mounted towards the front of the nacelle was programmed to measure the lateral velocity component with a horizontal, fixed beam at a 90° to the rotor axis (Fig. 3b, blue) for a period of 14 minutes. The time series of the lateral velocity $v(t)$ was extracted from the range gate at $y = 117$ m and low-pass filtered with a moving average using a window of $\frac{2D}{U_0}$. The short measurement distance leads to a high SNR, which causes the theoretical velocity uncertainty to be smaller than the velocity resolution of the instrument (0.038 m s^{-1}) [15]. Subsequently, the standard deviation of the lateral velocity ($\sigma_{v,f}$) and the lateral turbulence intensity ($TI_{v,f} = \frac{\sigma_{v,f}}{U_0}$) were computed from the measurements and assumed to be representative for the rotor area.

The rear-mounted Doppler LiDAR scanned the velocity field of the wake at hub height (Fig. 3b, red). It was programmed to perform 230 successive Plan Position Indicator (PPI) scans in the downstream direction with an opening angle of ±12° and an azimuth step of 2° to capture the wake. Each PPI took 7.2 s to complete including the return to the starting position and the full scan was completed in approximately 28.4 minutes. A signal-to-noise ratio (SNR) threshold of -14 dB was used, which leads to an upper bound of the theoretical velocity uncertainty of 0.3 m s^{-1} [15] and the spatial uncertainty due to the scanner movement is assumed to be equal to the azimuth step. The amplitude of the mean velocity deficit and the turbulence intensity added by wake meandering were derived from the wake scans following the post-processing, and data selection criteria described in [5]. Only the first half of the wake scans that coincides with the measurements of the front-mounted Doppler LiDAR are analysed for the comparison in Sect. 4.

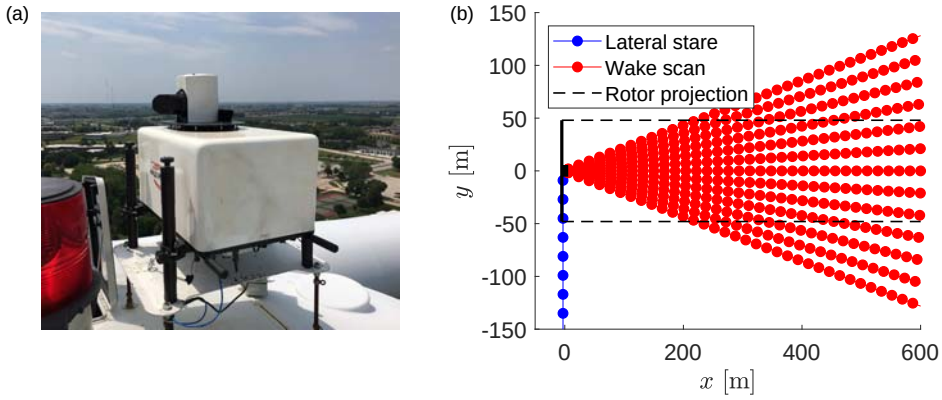

Figure 3. Photo of the front-mounted Doppler LiDAR on the nacelle of the wind turbine (a). The scan patterns of the nacelle mounted Doppler LiDARs viewed from top (b). Wake scans of the rear-mounted Doppler LiDAR (red) were accompanied by measurements in a lateral staring mode of the front-mounted Doppler LiDAR (blue). LiDAR beams are shown as lines with range gate centers indicated as points. The wind turbine and the projection of the rotor edge is shown in black dashed lines.

4. Results

The proposed SWM model will be compared to predictions of the DWM model and to observations of the wake scanning Doppler LiDAR for validation. The implementation of the DWM model is the same as in [6]. Both, the SWM model and the DWM model, were initialised with U_0 from the SCADA data and $v(t)$ from the front-mounted Doppler LiDAR. The data set for the validation comprises of 43 cases of inflow and wake measurements covering a wind speed range between 5 m s^{-1} and 11 m s^{-1}, and lateral turbulence intensities up to 8% (a more detailed characterization is provided in [5]). The validation will focus on $x = 5D$ where the scanning cone of the wake scanning Doppler LiDAR has a width of $2D$.

First, the amplitude of the mean velocity deficit predicted by the SWM model is validated. The results of the SWM model, the DWM model and the observations are shown in Fig. 4a-c. All three show a decrease of the normalized velocity deficit with TI_v. Agreement of the SWM model to the DWM model and to the observations is good for $TI_v > 0.04$, but the SWM model predicts a larger mean velocity deficit for $TI_v < 0.04$. The reason for this overestimation is that $x_{0,MFoR} > 5D$ for $TI_v < 0.04$ (not withstanding some variation due to the thrust coefficient) and the quasi-steady velocity deficit becomes unrealistic in the near-wake. The slope and intercept of a linear regression of the SWM model for $TI_v > 0.04$ agree within the the 95%-confidence bounds to the linear regressions of DWM model. The lower correlation coefficient of the observations in Fig. 4c can be explained by the already lower correlation coefficient between the wake meandering strength and the TI_v that is $r = 0.6$ [5].

To demonstrate the additional value that the SWM model provides over analytical wake models, the fraction of the velocity deficit recovery that is caused by wake meandering is investigated next (Fig. 4d-f). Both models and the observations show that the contribution of wake meandering to the velocity deficit recovery increases with TI_v. The slope of the linear regression of the SWM model agrees to the DWM model and the observations within the confidence bounds. The problems that the SWM model has with the quasi-steady velocity deficit in the near-wake do not affect this comparison strongly from which we interpret that the meandering distribution is realistic across the full range of TI_v. If the SWM model uses the same quasi-steady velocity deficit as the DWM model, the difference in slope reduces to 0.02.

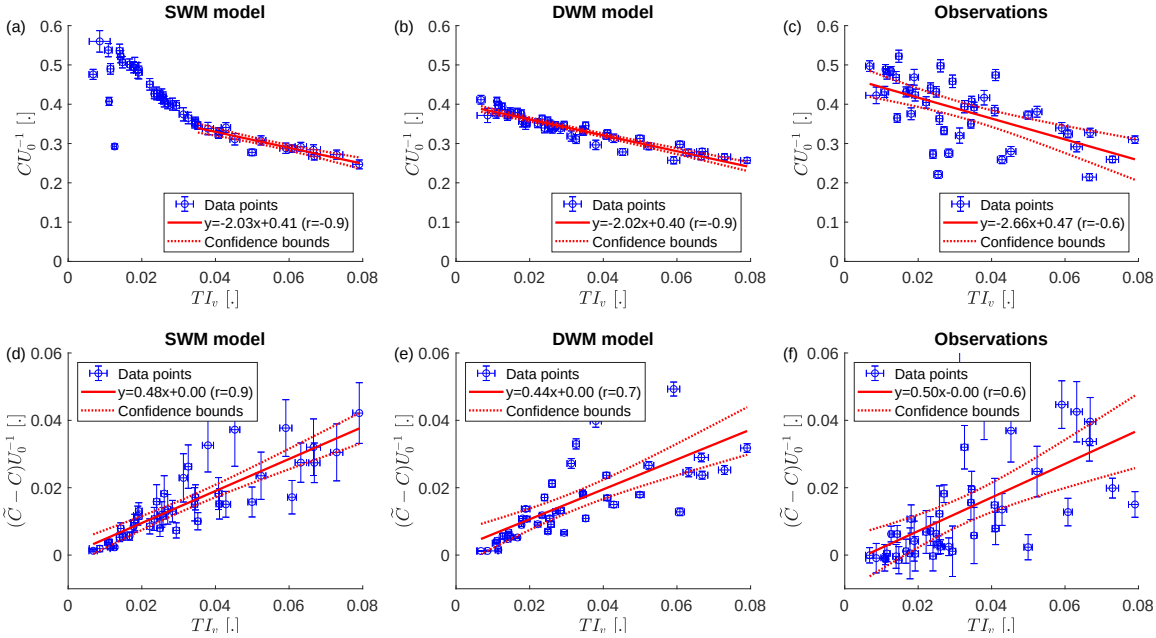

Figure 4. The upper row shows the normalized amplitude of the velocity deficit in the FFoR (C) as a function of the lateral turbulence intensity at $x = 5D$ for the proposed SWM model (a), the DWM model (b), and the observations of the wake scanning Doppler LiDAR (c). The bottom row shows the difference of velocity deficit amplitude between the MFoR and the FFoR ($\widetilde{C} - C$) for the proposed SWM model (d), the DWM model (e), and the observations of the wake scanning Doppler LiDAR (f). C is the maximum of ΔU_{avg} (Eq. 1) and $\widetilde{C}$ is the maximum of ΔU_{qs} (Eq. 6). A linear regression with the 95%-confidence bounds are shown in red (in case of panel (a) only $TI_v > 0.04$ is used for the regression). The error bars of the data points show the propagated errors based on the measurement uncertainties stated in Sect. 3 using a Monte-Carlo approach.

Lastly, the predictions for the added turbulence intensity due to wake meandering are validated. Both models and the observations show that $\langle TI_{added} \rangle$ increases with TI_v (Fig. 5). In a linear regression, the slope of the SWM model agrees within the confidence bounds to the DWM model and the observations. However, the intercept of the DWM model and the SWM model are significantly different from the observations, indicating that one of them is biased.

The distribution of $\langle TI_{added} \rangle$ as a function of x is shown in Fig. 6. This figure should be interpreted cautiously for several reasons. First, the scanning cone of the Doppler LiDAR increases in width with downstream distance while the spatial resolution decreases. This behaviour was replicated in the evaluation of the models for comparability, but it possibly biases the behaviour of $\langle TI_{added} \rangle$ with x compared to what would be observed with a constant domain and a constant spatial resolution. Second, we initialize the DWM model with a constant thrust coefficient along the radius. This makes the quasi-steady velocity deficit become more top-hat shaped for small x and the sharp velocity gradient at the edge inflates $\langle TI_{added} \rangle$ for the DWM model. This could possibly be improved by using a non-constant distribution of the thrust coefficient in the DWM model. The results show a decrease of $\langle TI_{added} \rangle$ with x for the SWM model and the observations. Similar to the results of Fig. 4, we observe a positive bias of the SWM model compared to the observations that exists across the whole range of x. A difference of $\langle TI_{added} \rangle$ between the SWM model and the DWM model reduces with x. Overall, the SWM model replicate the trends of the observations, but has a constant positive bias compared to the observations.

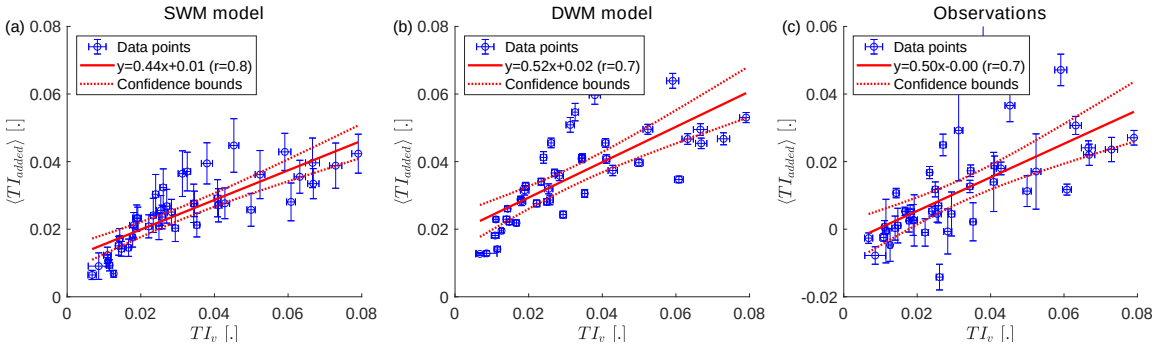

Figure 5. The added wake turbulence intensity due to wake meandering $\langle TI_{added} \rangle$ at $x = 5D$ as function of the lateral turbulence intensity of the inflow for the proposed SWM model (a), the DWM model (b), and the observations of the wake scanning Doppler LiDAR (c). For the SWM model and the DWM model, $\langle TI_{added} \rangle$ was quantified using Eq. (7) at grid points corresponding to the measurement points of the wake-scanning LiDAR and then laterally averaged across the scanning cone of the rear-mounted Doppler LiDAR. For the observations, $\langle TI_{added} \rangle$ was quantified as the laterally averaged difference in turbulence intensity between FFoR and MFoR [5]. A linear regression with the 95%-confidence bounds are shown in red. The error bars show the propagated errors based on the measurement uncertainties stated in Sect. 3 using a Monte-Carlo approach.

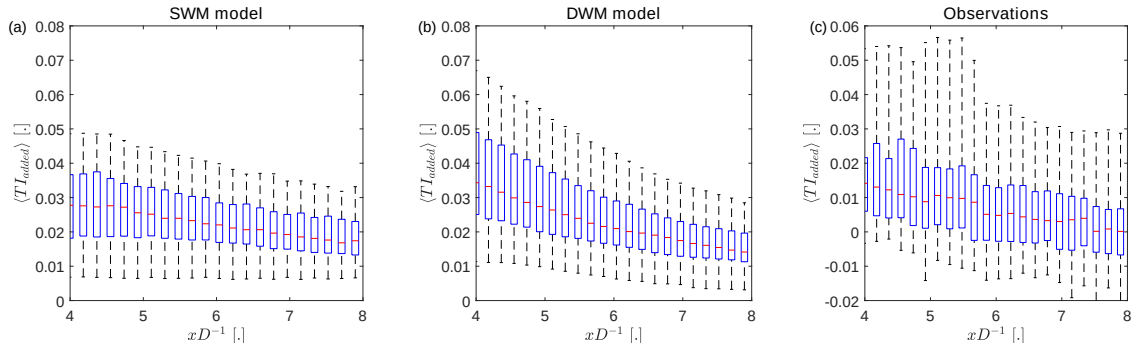

Figure 6. The added wake turbulence intensity due to wake meandering $\langle TI_{added} \rangle$ as a function of the downstream distance for the proposed SWM model (a), the DWM model (b), and the observations of the wake scanning Doppler LiDAR (c). Our implementation of the DWM model uses a constant thrust coefficient that negatively affects the results (see main text). The whiskers show the range of the data, blue bins the 25th and 75th percentile, and the red line the median value. The range of the data at each bin is explained by turbulence intensity, which can be seen for $x = 5D$ in Fig. 5.

5. Conclusions

A new statistical wake meandering (SWM) model has been proposed. Compared to previous SWM models, the proposed model has the benefit of a simple implementation, because it does not require look-up tables created from simulations, while at the same time being applicable to a wide range of flow conditions. The predictions of the proposed SWM model for the effect of wake meandering on the mean velocity field show agreement to the Dynamic Wake Meandering (DWM) model and to the observations of a wake scanning Doppler LiDAR at a utility-scale wind turbine in the far-wake. For the added turbulence intensity due to wake meandering, the SWM model shows agreement with the DWM model, but has a positive bias compared to the observations.

We consider the quasi-steady velocity deficit in the near-wake to be the weakest point of

the proposed SWM model. Improving it to be applicable in near-wake would be desirable to make the model viable for shorter turbine spacings, which is relevant for the modernization (repowering) of existing wind farms. Also, it is desirable to find a convolution-based expression for the added turbulence intensity instead of the ensemble standard deviation, which would improve the computation speed of the SWM model significantly. Lastly, a validation of the proposed SWM model with a reference data set from the Horns Rev and Lillgrund offshore wind farms [9] would be desirable for better comparison to existing SWM models that were validated on this data set.

References

[1] J. F. Ainslie. Calculating the flowfield in the wake of wind turbines. *J. Wind Eng. Ind. Aerod.*, 27(1):213–224, 1988.
[2] M. Bastankhah and F. Porté-Agel. A new analytical model for wind-turbine wakes. *Renew. Energy*, 70:116 – 123, 2014. Special issue on aerodynamics of offshore wind energy systems and wakes.
[3] F. Bingöl, J. Mann, and G. C. Larsen. Light detection and ranging measurements of wake dynamics part i: one-dimensional scanning. *Wind Energy*, 13(1):51–61, 2010.
[4] R. Braunbehrens and A. Segalini. A statistical model for wake meandering behind wind turbines. *J. Wind Eng. Ind. Aerod.*, 193:103954, 2019.
[5] P. Brugger, C. Markfort, and F. Porté-Agel. Field measurements of wake meandering at a utility-scale wind turbine with nacelle-mounted doppler lidars. *Wind Energy Science*, 7(1):185–199, 2022.
[6] P. Brugger, C. Markfort, and F. Porté-Agel. Improvements to the dynamic wake meandering model by incorporating the turbulent schmidt number. *Wind Energy Science Discussions*, 2023:1–28, 2023.
[7] F. C. Fuertes, C. Markfort, and F. Porté-Agel. Wind turbine wake characterization with nacelle-mounted wind lidars for analytical wake model validation. *Remote Sens.-Basel*, 10(5), 2018.
[8] E. T. Garcia, S. Aubrun, M. Boquet, P. Royer, O. Coupiac, and N. Girard. Wake meandering and its relationship with the incoming wind characteristics: a statistical approach applied to long-term on-field observations. *J Phys. Conf. Ser.*, 854:012045, may 2017.
[9] M. Gaumond, P.-E. Réthoré, A. Bechmann, S. Ott, G. C. Larsen, A. Peña, and Kurt S. Hansen. Benchmarking of wind turbine wake models in large offshore wind farms. In *Proceedings of the science of making torque from wind conference*, 2012.
[10] N. O. Jensen. *A note on wind generator interaction.* Number 2411 in Risø-M. Risø National Laboratory, 1983.
[11] R.-E. Keck. Validation of the standalone implementation of the dynamic wake meandering model for power production. *Wind Energy*, 18(9):1579–1591, 2015.
[12] R.-E. Keck, M. de Maré, M. J. Churchfield, S. Lee, G. Larsen, and H. A. Madsen. On atmospheric stability in the dynamic wake meandering model. *Wind Energy*, 17(11):1689–1710, 2014.
[13] G. C. Larsen, H. A. Madsen, K. Thomsen, and T. J. Larsen. Wake meandering: a pragmatic approach. *Wind Energy*, 11(4):377–395, 2008.
[14] E. Machefaux, G. C. Larsen, N. Troldborg, M. Gaunaa, and A. Rettenmeier. Empirical modeling of single-wake advection and expansion using full-scale pulsed lidar-based measurements. *Wind Energy*, 18(12):2085–2103, 2015.
[15] Guy Pearson, Fay Davies, and Chris Collier. An analysis of the performance of the ufam pulsed doppler lidar for observing the boundary layer. *J. Atmos. Ocean Tech.*, 26(2):240–250, 2009.
[16] I. Reinwardt, L. Schilling, P. Dalhoff, D. Steudel, and M. Breuer. Dynamic wake meandering model calibration using nacelle-mounted lidar systems. *Wind Energy Science*, 5(2):775–792, 2020.
[17] G. J. Taylor, D. J. Milborrow, D. N. McIntosh, and D. T. Swift-Hook. Wake measurements on the nibe windmills. In *Proceedings of Seventh BWEA Wind Energy Conference, Oxford*, pages 67–73, 1985.
[18] E. Thøgersen, B. Tranberg, J. Herp, and M. Greiner. Statistical meandering wake model and its application to yaw-angle optimisation of wind farms. In *J Phys. Conf. Ser.*, volume 854, page 012017. IOP Publishing, 2017.
[19] J.-J. Trujillo, F. Bingöl, G. C. Larsen, J. Mann, and M. Kühn. Light detection and ranging measurements of wake dynamics. part ii: two-dimensional scanning. *Wind Energy*, 14(1):61–75, 2011.